POLITECNICO DI TORINO
Repository ISTITUZIONALE

On the Low-Frequency Behavior of Vector Potential Integral Equations for Perfect Electrically Conducting Scatterers

Terms of use:

Publisher copyright

(Article begins on next page)

21 May 2024

Communication

On the Low-Frequency Behavior of Vector Potential Integral Equations for Perfect Electrically Conducting Scatterers

Rui Chen[ID], H. Arda Ulku[ID], Francesco P. Andriulli[ID], and Hakan Bagci[ID]

Abstract—Low-frequency behavior of vector potential integral equations (VPIEs) for perfect electrically conducting (PEC) scatterers is investigated. Two equation sets are considered: the first set (VPIE-1) enforces the tangential component of the vector potential on the scatterer surface to be zero and uses the fundamental field relationship on its normal component. The second set (VPIE-2) uses the same condition as VPIE-1 for the tangential component of the vector potential but enforces its divergence to be zero. In both the sets, unknowns are the electric current and the normal component of the vector potential on the scatterer surface and are expanded using the Rao–Wilton–Glisson (RWG) and pulse basis functions, respectively. To achieve a conforming discretization, RWG, scalar Buffa–Christiansen (BC), and pulse testing functions are used. Theoretical and numerical analyses of the resulting matrix systems show that the electric current obtained by solving VPIE-1 has the wrong frequency scaling and is inaccurate at low frequencies.

Index Terms—Loop–star decomposition, low-frequency behavior, low-frequency breakdown, low-frequency electromagnetic simulation, perfect electrically conducting (PEC) scatterer, vector potential integral equations (VPIEs).

I. INTRODUCTION

Time-harmonic (frequency-domain) electromagnetic scattering from a perfect electrically conducting (PEC) object is often analyzed by solving the field integral equations, e.g., electric field integral equation (EFIE) or magnetic field integral equation (MFIE). However, it is well-known that EFIE discretized using the Rao–Wilton–Glisson (RWG) functions [1] suffers from low-frequency and dense discretization breakdowns, i.e., the matrix system that arises from its discretization becomes ill-conditioned [2], [3]. On the other hand, discretization of MFIE using the RWG functions yields a well-conditioned matrix system regardless of the frequency, but the solution of this matrix system is inaccurate at low frequencies [4], [5], [6], [7]. In the past few decades, many methods have been proposed to address these problems associated with the field integral equations. These methods include Helmholtz decomposition [8], [9], [10], [11], [12], preconditioning techniques [13], [14], [15], [16], [17], [18], mixed discretization schemes [5], [6], [7], and the formulation of new integral equations where electric charge density is defined as one of

the unknowns to be solved for [19], [20], [21], and [22]. However, these methods call for complicated discretization schemes [5], [6], [7], [8], [9], [10], [11], [12], [16], [17], [18], implementations that rely on perturbation analysis to address inaccuracy issues [18], [21], and specific excitation formulations [19], and/or come with higher computational requirements.

Recently, potential integral equations [23], [24], [25], [26], [27], [28], [29], [30], [31], [32] have been proposed as alternatives to the field integral equations for analyzing low-frequency electromagnetic scattering problems. In [24] and [25], formulations of different potential integral equations for dielectric and PEC scatterers are derived using the equivalence principle and the generalized Green theorem. These equations impose the continuity of the tangential and normal components of the vector potential on the scatterer surface and define the electric current and the normal component of the vector potential on the same surface as the unknowns to be solved for. The potential integral equations proposed in [26] rely on the formulation from [24] but they enforce the tangential component and the divergence of the vector potential on the scatterer surface. These equations are free from an apparent low-frequency breakdown, but the efficient iterative solution of the matrix system resulting from their discretization calls for a special preconditioner (due to the presence of a saddle point problem as the frequency approaches zero). This iterative solution often converges faster than the solution of the matrix system resulting from the discretization of the augmented EFIE [20] at low frequencies and/or for densely discretized surfaces. The formulation in [28] starts with the potential equations introduced in [26] but introduces an additional equation which has the normal component of the gradient of the scalar potential on the scatterer surface as the unknown. This additional equation helps compute the electric field in the near-field region more accurately at low frequencies.

In [27], a more generalized approach to derive potential integral equations for dielectric scatterers is described. Four different traces of the vector potential, namely, tangential component of curl of the vector potential, tangential component of the vector potential (same as the one in [24], [25], and [26]), normal component of the vector potential (same as the one in [24] and [25]), and divergence of the vector potential (same as the one in [26]), are used to derive four different integral equations in unknowns electric current and normal component of the vector potential on the scatterer surface. These two unknowns can be obtained by solving any combination of two of these integral equations. Note that for the specific vector potential integral equation (VPIE) formulation in [27], the first one of the four equations (the one obtained using the trace of the tangential component of curl of the vector potential) is MFIE (in only electric current), which is decoupled from the other three equations.

In this work, the low-frequency behavior of VPIEs for PEC scatterers is investigated. Since the solution of MFIE discretized using the RWG functions is inaccurate at low frequencies, any choice of combinations that includes MFIE is also expected to suffer from the same problem. Therefore, two sets of VPIEs that do not include MFIE are studied here. The first set includes the two equations obtained using the tangential and normal components of the vector

potential [25] (this set is termed as VPIE-1), and the second set includes the two equations obtained using the tangential component and the divergence of the vector potential [26] (this set is termed as VPIE-2).

To numerically investigate the low-frequency problem, the electric current and the normal component of the vector potential are expanded using the RWG and pulse basis functions, respectively, and these expansions are inserted into VPIE-1 and VPIE-2. To obtain a conformal discretization, VPIE-1 is tested using the RWG and scalar Buffa–Christiansen (BC) functions [14], [31], and VPIE-2 is tested using the RWG and pulse functions. The resulting matrix systems are then solved for the unknown expansion coefficients. To analyze the frequency behavior of the solutions of VPIE-1 and VPIE-2, loop–star decomposition [8] is used. This analysis and the numerical experiments, which are carried out for two different vector and scalar potential representations of the incident wave [23], show that the electric current solution of VPIE-1 is inaccurate at low frequencies; more specifically, it scales with the incorrect frequency dependence as the frequency approaches zero. Note that a preliminary version of this work is presented in a conference contribution [32].

II. FORMULATION

A. Vector Potential Integral Equation

Let Γ represent the (closed) surface of a PEC object that resides in an unbounded homogeneous background medium with permittivity ε_0 and permeability μ_0. The time dependence $e^{j\omega t}$ is assumed for all the sources, fields, and potentials. An electric field $\mathbf{E}^{\text{inc}}(\mathbf{r})$, which is characterized by the vector potential $\mathbf{A}^{\text{inc}}(\mathbf{r})$ and scalar potential $\Phi^{\text{inc}}(\mathbf{r})$, is incident on Γ. Upon this excitation, Γ supports the surface electric current $\mathbf{J}(\mathbf{r}) = \hat{\mathbf{n}}(\mathbf{r}) \times \nabla \times \mathbf{A}(\mathbf{r})/\mu_0$. Here, $\mathbf{A}(\mathbf{r}) = \mathbf{A}^{\text{sca}}(\mathbf{r}) + \mathbf{A}^{\text{inc}}(\mathbf{r})$ is the total vector potential, $\mathbf{A}^{\text{sca}}(\mathbf{r})$ is the scattered vector potential, and $\hat{\mathbf{n}}(\mathbf{r})$ is the outward pointing unit vector at $\mathbf{r}$ on Γ. On Γ, $\hat{\mathbf{n}}(\mathbf{r}) \times \mathbf{A}(\mathbf{r}) = 0$ and $\nabla \cdot \mathbf{A}(\mathbf{r}) = 0$. $\mathbf{A}^{\text{sca}}(\mathbf{r})$ can be represented as [24], [26], [27]

$$\mathbf{A}^{\text{sca}}(\mathbf{r}) = S[\mu_0 \mathbf{J}](\mathbf{r}) - \nabla S[\hat{\mathbf{n}} \cdot \mathbf{A}](\mathbf{r}) \tag{1}$$

where

$$S[X] = \int_\Gamma G(\mathbf{r}, \mathbf{r}') X(\mathbf{r}') ds'$$

$G(\mathbf{r}, \mathbf{r}') = e^{-jk_0|\mathbf{r}-\mathbf{r}'|}/(4\pi|\mathbf{r}-\mathbf{r}'|)$ is the Green function, and $k_0 = \omega\sqrt{\mu_0\varepsilon_0}$ is the wavenumber in the background medium. Inserting (1) into

$$\hat{\mathbf{n}}(\mathbf{r}) \times \nabla \times \mathbf{A}(\mathbf{r}) = \hat{\mathbf{n}}(\mathbf{r}) \times \nabla \times \mathbf{A}^{\text{sca}}(\mathbf{r}) + \hat{\mathbf{n}}(\mathbf{r}) \times \nabla \times \mathbf{A}^{\text{inc}}(\mathbf{r})$$

$$\hat{\mathbf{n}}(\mathbf{r}) \times \mathbf{A}(\mathbf{r}) = \hat{\mathbf{n}}(\mathbf{r}) \times \mathbf{A}^{\text{sca}}(\mathbf{r}) + \hat{\mathbf{n}}(\mathbf{r}) \times \mathbf{A}^{\text{inc}}(\mathbf{r}) = 0$$

$$\hat{\mathbf{n}}(\mathbf{r}) \cdot \mathbf{A}(\mathbf{r}) = \hat{\mathbf{n}}(\mathbf{r}) \cdot \mathbf{A}^{\text{sca}}(\mathbf{r}) + \hat{\mathbf{n}}(\mathbf{r}) \cdot \mathbf{A}^{\text{inc}}(\mathbf{r})$$

$$\nabla \cdot \mathbf{A}(\mathbf{r}) = \nabla \cdot \mathbf{A}^{\text{sca}}(\mathbf{r}) + \nabla \cdot \mathbf{A}^{\text{inc}}(\mathbf{r}) = 0$$

for $\mathbf{r} \in \Gamma$ yields four VPIEs in unknowns $\mathbf{J}(\mathbf{r})$ and $\hat{\mathbf{n}}(\mathbf{r}) \cdot \mathbf{A}(\mathbf{r})$ [27]

$$\mu_0 \mathbf{J}(\mathbf{r}) - \hat{\mathbf{n}}(\mathbf{r}) \times \nabla \times S[\mu_0 \mathbf{J}](\mathbf{r})$$
$$= \hat{\mathbf{n}}(\mathbf{r}) \times \nabla \times \mathbf{A}^{\text{inc}}(\mathbf{r}) \tag{2}$$

$$\hat{\mathbf{n}}(\mathbf{r}) \times S[\mu_0 \mathbf{J}](\mathbf{r}) - \hat{\mathbf{n}}(\mathbf{r}) \times \nabla S[\hat{\mathbf{n}} \cdot \mathbf{A}](\mathbf{r})$$
$$= -\hat{\mathbf{n}}(\mathbf{r}) \times \mathbf{A}^{\text{inc}}(\mathbf{r}) \tag{3}$$

$$-\frac{1}{2}\hat{\mathbf{n}}(\mathbf{r}) \cdot \mathbf{A}(\mathbf{r}) + \hat{\mathbf{n}}(\mathbf{r}) \cdot S[\mu_0 \mathbf{J}](\mathbf{r}) - \hat{\mathbf{n}}(\mathbf{r}) \cdot \nabla S[\hat{\mathbf{n}} \cdot \mathbf{A}](\mathbf{r})$$
$$= -\hat{\mathbf{n}}(\mathbf{r}) \cdot \mathbf{A}^{\text{inc}}(\mathbf{r}) \tag{4}$$

$$\nabla \cdot S[\mu_0 \mathbf{J}](\mathbf{r}) + k_0^2 S[\hat{\mathbf{n}} \cdot \mathbf{A}](\mathbf{r})$$
$$= -\nabla \cdot \mathbf{A}^{\text{inc}}(\mathbf{r}). \tag{5}$$

Note that in (5), $\nabla \cdot \nabla S[\hat{\mathbf{n}} \cdot \mathbf{A}](\mathbf{r}) = \nabla^2 S[\hat{\mathbf{n}} \cdot \mathbf{A}](\mathbf{r})$ is replaced by $-k_0^2 S[\hat{\mathbf{n}} \cdot \mathbf{A}](\mathbf{r})$ using the Helmholtz equation [26].

To solve for two unknowns, $\mathbf{J}(\mathbf{r})$ and $\hat{\mathbf{n}}(\mathbf{r}) \cdot \mathbf{A}(\mathbf{r})$, one has to choose one equation from (2) and (3) and another equation from (4) and (5) [27]. Note that (2) is MFIE [in only one unknown $\mathbf{J}(\mathbf{r})$] and decoupled from (3)–(5), and it is clear that any equation set that

includes (2) suffers from the inaccuracy problems that MFIE has at low frequencies [4], [5], [6], [7]. In this work, two equation sets that do not include (2) are studied. The first equation set includes (3) and (4) and is termed as "VPIE-1" [25]. VPIE-1 does not have any explicit dependence on the frequency, but its solution becomes inaccurate at low frequencies with an RWG-based discretization. The second equation set includes (3) and (5) and is termed as "VPIE-2" [26]. VPIE-2 depends explicitly on frequency via k_0^2, but its RWG-based discretization yields an accurate solution at low frequencies.

B. Discretization

To numerically solve VPIE-1 and VPIE-2, first, Γ is discretized into a mesh of triangles denoted by Γ^{h}. The unknowns $\mathbf{J}(\mathbf{r})$ and $\hat{\mathbf{n}}(\mathbf{r}) \cdot \mathbf{A}(\mathbf{r})$ belong to the Sobolev spaces $\mathbb{H}^{-1/2}_{\text{div}}(\Gamma)$ and $\mathcal{H}^{-1/2}(\Gamma)$, respectively [5], [6], [7], [14], [31]. Therefore, they are expanded using the RWG basis functions $\mathbf{f}^{\text{R}}_n(\mathbf{r})$ [1] [that reside in $\mathbb{H}^{-1/2}_{\text{div}}(\Gamma^{\text{h}})$] and pulse basis functions $f^{\text{P}}_n(\mathbf{r})$ [29] [that reside in $\mathcal{H}^{-1/2}(\Gamma^{\text{h}})$], respectively,

$$\mu_0 \mathbf{J}(\mathbf{r}) = \sum_{n=1}^{N_{\text{R}}} \{\mathbf{I}_{\text{R}}\}_n \mathbf{f}^{\text{R}}_n(\mathbf{r}) \tag{6}$$

$$\hat{\mathbf{n}}(\mathbf{r}) \cdot \mathbf{A}(\mathbf{r}) = \sum_{n=1}^{N_{\text{P}}} \{\mathbf{I}_{\text{P}}\}_n f^{\text{P}}_n(\mathbf{r}). \tag{7}$$

Here, N_{R} and N_{P} are the numbers of edges and triangular patches, respectively, and $\mathbf{I}_{\text{R}}$ and $\mathbf{I}_{\text{P}}$ are the vectors that store the unknown expansion coefficients of $\mathbf{f}^{\text{R}}_n(\mathbf{r})$ and $f^{\text{P}}_n(\mathbf{r})$, respectively. As explained in [5], [6], [7], [31], and [14], the testing function should reside in the dual space of the range of the integral operator. Considering the mapping properties of the integral operators in (3)–(5) [31] and the basis functions used in (6) and (7), it can be shown that the range spaces for (3)–(5) are $\mathbb{H}^{-1/2}_{\text{div}}(\Gamma)$, $\mathcal{H}^{-1/2}(\Gamma)$, and $\mathcal{H}^{1/2}(\Gamma)$, respectively. Therefore, the functions used for testing (3)–(5) should reside in their dual spaces, namely, $\mathbb{H}^{-1/2}_{\text{curl}}(\Gamma^{\text{h}})$, $\mathcal{H}^{1/2}(\Gamma^{\text{h}})$, and $\mathcal{H}^{-1/2}(\Gamma^{\text{h}})$, respectively [31]. This means that to obtain a conforming discretization, the rotated RWG function $\hat{\mathbf{n}}(\mathbf{r}) \times \mathbf{f}^{\text{R}}_m(\mathbf{r})$, scalar BC function $f^{\text{B}}_m(\mathbf{r})$ [14], [31], and pulse function $f^{\text{P}}_m(\mathbf{r})$ can be used to test (3)–(5), respectively.

Inserting (6) and (7) into (3) and (4) (VPIE-1) and (3)–(5) (VPIE-2) and testing the resulting equations with $\hat{\mathbf{n}}(\mathbf{r}) \times \mathbf{f}^{\text{R}}_m(\mathbf{r})$, $m = 1, 2, \ldots, N_{\text{R}}$, $f^{\text{B}}_m(\mathbf{r})$, $m = 1, 2, \ldots, N_{\text{P}}$, and $f^{\text{P}}_m(\mathbf{r})$, $m = 1, 2, \ldots, N_{\text{P}}$ yield the matrix system

$$\begin{bmatrix} \mathbf{Z}_{\text{RR}} & \mathbf{Z}_{\text{RP}} \\ \mathbf{Z}_{\text{PR}} & \mathbf{Z}_{\text{PP}} \end{bmatrix} \begin{bmatrix} \mathbf{I}_{\text{R}} \\ \mathbf{I}_{\text{P}} \end{bmatrix} = \begin{bmatrix} \mathbf{V}_{\text{R}} \\ \mathbf{V}_{\text{P}} \end{bmatrix}. \tag{8}$$

Here, the entries of the matrix blocks $\mathbf{Z}_{\text{RR}}$, $\mathbf{Z}_{\text{RP}}$, $\mathbf{Z}_{\text{PR}}$, and $\mathbf{Z}_{\text{PP}}$ are given by

$$\{\mathbf{Z}_{\text{RR}}\}_{mn} = \left\langle \hat{\mathbf{n}}(\mathbf{r}) \times \mathbf{f}^{\text{R}}_m(\mathbf{r}), \hat{\mathbf{n}}(\mathbf{r}) \times S[\mathbf{f}^{\text{R}}_n](\mathbf{r}) \right\rangle$$
$$= \int_{\Gamma^{\text{R}}_m} \mathbf{f}^{\text{R}}_m(\mathbf{r}) \cdot \int_{\Gamma^{\text{R}}_n} G(\mathbf{r}, \mathbf{r}') \mathbf{f}^{\text{R}}_n(\mathbf{r}') ds' ds \tag{9}$$

$$\{\mathbf{Z}_{\text{RP}}\}_{mn} = \left\langle \hat{\mathbf{n}}(\mathbf{r}) \times \mathbf{f}^{\text{R}}_m(\mathbf{r}), -\hat{\mathbf{n}}(\mathbf{r}) \times \nabla S[f^{\text{P}}_n](\mathbf{r}) \right\rangle$$
$$= \int_{\Gamma^{\text{R}}_m} \nabla \cdot \mathbf{f}^{\text{R}}_m(\mathbf{r}) \int_{\Gamma^{\text{P}}_n} G(\mathbf{r}, \mathbf{r}') f^{\text{P}}_n(\mathbf{r}') ds' ds \tag{10}$$

VPIE-1: $\{\mathbf{Z}_{\text{PR}}\}_{mn} = \left\langle f^{\text{B}}_m(\mathbf{r}), \hat{\mathbf{n}}(\mathbf{r}) \cdot S[\mathbf{f}^{\text{R}}_n](\mathbf{r}) \right\rangle$
$$= \int_{\Gamma^{\text{B}}_m} f^{\text{B}}_m(\mathbf{r}) \int_{\Gamma^{\text{R}}_n} G(\mathbf{r}, \mathbf{r}') \hat{\mathbf{n}}(\mathbf{r}) \cdot \mathbf{f}^{\text{R}}_n(\mathbf{r}') ds' ds$$

VPIE-2: $\{\mathbf{Z}_{\text{PR}}\}_{mn} = \left\langle f^{\text{P}}_m(\mathbf{r}), \nabla \cdot S[\mathbf{f}^{\text{R}}_n](\mathbf{r}) \right\rangle$
$$= \int_{\Gamma^{\text{P}}_m} f^{\text{P}}_m(\mathbf{r}) \int_{\Gamma^{\text{R}}_n} G(\mathbf{r}, \mathbf{r}') \nabla' \cdot \mathbf{f}^{\text{R}}_n(\mathbf{r}') ds' ds \tag{11}$$

VPIE-1: $\{\mathbf{Z}_{PP}\}_{mn} = \left\langle f_m^B(\mathbf{r}), -\frac{1}{2}f_n^P(\mathbf{r}) - \hat{\mathbf{n}}(\mathbf{r}) \cdot \nabla S[f_n^P](\mathbf{r}) \right\rangle$

$$= -\frac{1}{2}\int_{\Gamma_m^B} f_m^B(\mathbf{r})f_n^P(\mathbf{r})ds$$

$$+ \int_{\Gamma_m^B} f_m^B(\mathbf{r})\int_{\Gamma_n^P}\hat{\mathbf{n}}(\mathbf{r})\cdot\nabla'G(\mathbf{r},\mathbf{r}')f_n^P(\mathbf{r}')ds'ds$$

VPIE-2: $\{\mathbf{Z}_{PP}\}_{mn} = \left\langle f_m^P(\mathbf{r}), k_0^2 S[f_n^P](\mathbf{r}) \right\rangle$

$$= k_0^2\int_{\Gamma_m^P} f_m^P(\mathbf{r})\int_{\Gamma_n^P}G(\mathbf{r},\mathbf{r}')f_n^P(\mathbf{r}')ds'ds \quad (12)$$

and the entries of the vectors $\mathbf{V}_R$ and $\mathbf{V}_P$ are given by

$$\{\mathbf{V}_R\}_m = \left\langle \hat{\mathbf{n}}(\mathbf{r})\times\mathbf{f}_m^R(\mathbf{r}), -\hat{\mathbf{n}}(\mathbf{r})\times\mathbf{A}^{inc}(\mathbf{r}) \right\rangle$$

$$= -\int_{\Gamma_m^R}\mathbf{f}_m^R(\mathbf{r})\cdot\mathbf{A}^{inc}(\mathbf{r})ds \quad (13)$$

VPIE-1: $\{\mathbf{V}_P\}_m = \left\langle f_m^B(\mathbf{r}), -\hat{\mathbf{n}}(\mathbf{r})\cdot\mathbf{A}^{inc}(\mathbf{r}) \right\rangle$

$$= -\int_{\Gamma_m^B}f_m^B(\mathbf{r})\hat{\mathbf{n}}(\mathbf{r})\cdot\mathbf{A}^{inc}(\mathbf{r})ds$$

VPIE-2: $\{\mathbf{V}_P\}_m = \left\langle f_m^P(\mathbf{r}), -\nabla\cdot\mathbf{A}^{inc}(\mathbf{r}) \right\rangle$

$$= j\omega\mu_0\varepsilon_0\int_{\Gamma_m^P}f_m^P(\mathbf{r})\Phi^{inc}(\mathbf{r})ds. \quad (14)$$

Here, Γ_m^R, Γ_m^B, and Γ_m^P denote the support of $\mathbf{f}_m^R(\mathbf{r})$, $f_m^B(\mathbf{r})$, and $f_m^P(\mathbf{r})$, respectively. Note that in (14), the Lorenz gauge $\nabla\cdot\mathbf{A}^{inc}(\mathbf{r}) = -j\omega\mu_0\varepsilon_0\Phi^{inc}(\mathbf{r})$ is used [23], [24]. Two kinds of vector and scalar potential representations of the plane-wave excitation are considered in this work. For the first representation, $\mathbf{A}_1^{inc}(\mathbf{r}) = 1/(-j\omega)\mathbf{E}^{inc}(\mathbf{r})$ and $\Phi_1^{inc}(\mathbf{r}) = 0$ [26]. This representation does not lead to a stable uncoupling of the potentials since $\mathbf{A}_1^{inc}(\mathbf{r})$ is unbounded as $\omega \to 0$ [23]. For the second representation, $\mathbf{A}_2^{inc}(\mathbf{r}) = -\sqrt{\mu_0\varepsilon_0}\hat{\mathbf{k}}^{inc}[\mathbf{r}\cdot\mathbf{E}^{inc}(\mathbf{r})]$ and $\Phi_2^{inc}(\mathbf{r}) = -\mathbf{r}\cdot\mathbf{E}^{inc}(\mathbf{r})$, where $\hat{\mathbf{k}}^{inc}$ represents the direction of propagation [23]. This representation yields potentials that satisfy the Lorenz gauge and are bounded as $\omega \to 0$ [23].

C. Comments

For VPIE-2, the matrix system (8) has a saddle point problem at low frequencies [26], [33]. Therefore, for its efficient iterative solution, one has to use a special preconditioner [26], [33]. Note that even though it is not discussed in [26], the construction of this preconditioner is not trivial at very low frequencies: One of its diagonal blocks behaves like a (discretized) Laplacian operator and has an isolated zero eigenvalue [20], [21], [34]. Since this work focuses on the accuracy of VPIE-1 and VPIE-2 at low frequencies (rather than their efficient solution), matrix system (8) is solved using LU decomposition. However, as $\omega \to 0$, the VPIE-2's matrix system has one isolated eigenvalue that approaches zero (due to charge neutrality/redundancy [20], [21]). Therefore, a matrix deflation method is applied [20] before LU decomposition is used.

D. Low-Frequency Analysis

To investigate the accuracy of VPIE-1 and VPIE-2 as $\omega \to 0$, $\mathbf{J}(\mathbf{r})$ is separated into its solenoidal and non-solenoidal components using loop–star decomposition as [8]

$$\mu_0\mathbf{J}(\mathbf{r}) = \sum_{n=1}^{N_L}\{\mathbf{I}_L\}_n\mathbf{f}_n^L(\mathbf{r}) + \sum_{n=1}^{N_S}\{\mathbf{I}_S\}_n\mathbf{f}_n^S(\mathbf{r}). \quad (15)$$

Here, $N_S = N_P - 1 = N_R - N_L$, $\mathbf{f}_n^L(\mathbf{r})$ and $\mathbf{f}_n^S(\mathbf{r})$ are the loop and the star basis functions, respectively, and $\mathbf{I}_L$ and $\mathbf{I}_S$ are the vectors that store their coefficients, respectively. Inserting (15) and (7) into (3)–(5) and testing the resulting equations with $\hat{\mathbf{n}}(\mathbf{r})\times\mathbf{f}_m^L(\mathbf{r})$,

$m = 1, 2, \ldots, N_L$, $\hat{\mathbf{n}}(\mathbf{r})\times\mathbf{f}_m^S(\mathbf{r})$, $m = 1, 2, \ldots, N_S$, $f_m^B(\mathbf{r})$, $m = 1, 2, \ldots, N_P$, and $f_m^P(\mathbf{r})$, $m = 1, 2, \ldots, N_P$ yield

$$\begin{bmatrix} \mathbf{Z}_{LL} & \mathbf{Z}_{LS} & \mathbf{Z}_{LP} \\ \mathbf{Z}_{SL} & \mathbf{Z}_{SS} & \mathbf{Z}_{SP} \\ \mathbf{Z}_{PL} & \mathbf{Z}_{PS} & \mathbf{Z}_{PP} \end{bmatrix}\begin{bmatrix} \mathbf{I}_L \\ \mathbf{I}_S \\ \mathbf{I}_P \end{bmatrix} = \begin{bmatrix} \mathbf{V}_L \\ \mathbf{V}_S \\ \mathbf{V}_P \end{bmatrix}. \quad (16)$$

Here, the entries of the matrix blocks $\mathbf{Z}_{MN}$, M, N $\in$ {S, L, P} are given by

$$\{\mathbf{Z}_{LL}\}_{mn} = \left\langle \hat{\mathbf{n}}(\mathbf{r})\times\mathbf{f}_m^L(\mathbf{r}), \hat{\mathbf{n}}(\mathbf{r})\times S[\mathbf{f}_n^L](\mathbf{r}) \right\rangle$$

$$= \int_{\Gamma_m^L}\mathbf{f}_m^L(\mathbf{r})\cdot\int_{\Gamma_n^L}G(\mathbf{r},\mathbf{r}')\mathbf{f}_n^L(\mathbf{r}')ds'ds \quad (17)$$

$$\{\mathbf{Z}_{LS}\}_{mn} = \left\langle \hat{\mathbf{n}}(\mathbf{r})\times\mathbf{f}_m^L(\mathbf{r}), \hat{\mathbf{n}}(\mathbf{r})\times S[\mathbf{f}_n^S](\mathbf{r}) \right\rangle$$

$$= \int_{\Gamma_m^L}\mathbf{f}_m^L(\mathbf{r})\cdot\int_{\Gamma_n^S}G(\mathbf{r},\mathbf{r}')\mathbf{f}_n^S(\mathbf{r}')ds'ds \quad (18)$$

$$\{\mathbf{Z}_{LP}\}_{mn} = \left\langle \hat{\mathbf{n}}(\mathbf{r})\times\mathbf{f}_m^L(\mathbf{r}), -\hat{\mathbf{n}}(\mathbf{r})\times\nabla S[f_n^P](\mathbf{r}) \right\rangle$$

$$= \int_{\Gamma_m^L}\nabla\cdot\mathbf{f}_m^L(\mathbf{r})\int_{\Gamma_n^P}G(\mathbf{r},\mathbf{r}')f_n^P(\mathbf{r}')ds'ds \quad (19)$$

$$\{\mathbf{Z}_{SL}\}_{mn} = \left\langle \hat{\mathbf{n}}(\mathbf{r})\times\mathbf{f}_m^S(\mathbf{r}), \hat{\mathbf{n}}(\mathbf{r})\times S[\mathbf{f}_n^L](\mathbf{r}) \right\rangle$$

$$= \int_{\Gamma_m^S}\mathbf{f}_m^S(\mathbf{r})\cdot\int_{\Gamma_n^L}G(\mathbf{r},\mathbf{r}')\mathbf{f}_n^L(\mathbf{r}')ds'ds \quad (20)$$

$$\{\mathbf{Z}_{SS}\}_{mn} = \left\langle \hat{\mathbf{n}}(\mathbf{r})\times\mathbf{f}_m^S(\mathbf{r}), \hat{\mathbf{n}}(\mathbf{r})\times S[\mathbf{f}_n^S](\mathbf{r}) \right\rangle$$

$$= \int_{\Gamma_m^S}\mathbf{f}_m^S(\mathbf{r})\cdot\int_{\Gamma_n^S}G(\mathbf{r},\mathbf{r}')\mathbf{f}_n^S(\mathbf{r}')ds'ds \quad (21)$$

$$\{\mathbf{Z}_{SP}\}_{mn} = \left\langle \hat{\mathbf{n}}(\mathbf{r})\times\mathbf{f}_m^S(\mathbf{r}), -\hat{\mathbf{n}}(\mathbf{r})\times\nabla S[f_n^P](\mathbf{r}) \right\rangle$$

$$= \int_{\Gamma_m^S}\nabla\cdot\mathbf{f}_m^S(\mathbf{r})\int_{\Gamma_n^P}G(\mathbf{r},\mathbf{r}')f_n^P(\mathbf{r}')ds'ds \quad (22)$$

VPIE-1: $\{\mathbf{Z}_{PL}\}_{mn} = \left\langle f_m^B(\mathbf{r}), \hat{\mathbf{n}}(\mathbf{r})\cdot S[\mathbf{f}_n^L](\mathbf{r}) \right\rangle$

$$= \int_{\Gamma_m^B}f_m^B(\mathbf{r})\int_{\Gamma_n^L}G(\mathbf{r},\mathbf{r}')\hat{\mathbf{n}}(\mathbf{r})\cdot\mathbf{f}_n^L(\mathbf{r}')ds'ds$$

VPIE-2: $\{\mathbf{Z}_{PL}\}_{mn} = \left\langle f_m^P(\mathbf{r}), \nabla\cdot S[\mathbf{f}_n^L](\mathbf{r}) \right\rangle$

$$= \int_{\Gamma_m^P}f_m^P(\mathbf{r})\int_{\Gamma_n^L}G(\mathbf{r},\mathbf{r}')\nabla'\cdot\mathbf{f}_n^L(\mathbf{r}')ds'ds \quad (23)$$

VPIE-1: $\{\mathbf{Z}_{PS}\}_{mn} = \left\langle f_m^B(\mathbf{r}), \hat{\mathbf{n}}(\mathbf{r})\cdot S[\mathbf{f}_n^S](\mathbf{r}) \right\rangle$

$$= \int_{\Gamma_m^B}f_m^B(\mathbf{r})\int_{\Gamma_n^S}G(\mathbf{r},\mathbf{r}')\hat{\mathbf{n}}(\mathbf{r})\cdot\mathbf{f}_n^S(\mathbf{r}')ds'ds$$

VPIE-2: $\{\mathbf{Z}_{PS}\}_{mn} = \left\langle f_m^P(\mathbf{r}), \nabla\cdot S[\mathbf{f}_n^S](\mathbf{r}) \right\rangle$

$$= \int_{\Gamma_m^P}f_m^P(\mathbf{r})\int_{\Gamma_n^S}G(\mathbf{r},\mathbf{r}')\nabla'\cdot\mathbf{f}_n^S(\mathbf{r}')ds'ds \quad (24)$$

and the entries of the vectors $\mathbf{V}_L$ and $\mathbf{V}_S$ are given by

$$\{\mathbf{V}_L\}_m = \left\langle \hat{\mathbf{n}}(\mathbf{r})\times\mathbf{f}_m^L(\mathbf{r}), -\hat{\mathbf{n}}(\mathbf{r})\times\mathbf{A}^{inc}(\mathbf{r}) \right\rangle$$

$$= -\int_{\Gamma_m^L}\mathbf{f}_m^L(\mathbf{r})\cdot\mathbf{A}^{inc}(\mathbf{r})ds \quad (25)$$

$$\{\mathbf{V}_S\}_m = \left\langle \hat{\mathbf{n}}(\mathbf{r})\times\mathbf{f}_m^S(\mathbf{r}), -\hat{\mathbf{n}}(\mathbf{r})\times\mathbf{A}^{inc}(\mathbf{r}) \right\rangle$$

$$= -\int_{\Gamma_m^S}\mathbf{f}_m^S(\mathbf{r})\cdot\mathbf{A}^{inc}(\mathbf{r})ds \quad (26)$$

where Γ_n^L and Γ_n^S denote the support of loop and star functions, respectively. Note that the entries of $\mathbf{Z}_{PP}$ and $\mathbf{V}_P$ are already provided in (12) and (14), respectively. In (19) and (23), $\nabla\cdot\mathbf{f}_m^L(\mathbf{r}) = 0$ and $\nabla'\cdot\mathbf{f}_n^L(\mathbf{r}') = 0$, respectively [8]. This ensures that $\mathbf{Z}_{LP} = 0$ for both VPIE-1 and VPIE-2, and $\mathbf{Z}_{PL} = 0$ for VPIE-2.

The frequency scaling of $\mathbf{I}_L$, $\mathbf{I}_S$, and $\mathbf{I}_P$ as $\omega \to 0$ can be derived from the scaling of all the matrix blocks and excitation vectors

in (16). Note that the Green function and its gradient present in the expressions of the entries of these matrix blocks scale with $\mathcal{O}(1)$ as $\omega \to 0$ [4], [18]. This means that the blocks of the matrix in (16) scale as

$$\text{VPIE-1:} \begin{bmatrix} \mathbf{Z}_{LL} & \mathbf{Z}_{LS} & \mathbf{Z}_{LP} \\ \mathbf{Z}_{SL} & \mathbf{Z}_{SS} & \mathbf{Z}_{SP} \\ \mathbf{Z}_{PL} & \mathbf{Z}_{PS} & \mathbf{Z}_{PP} \end{bmatrix} = \begin{bmatrix} \mathcal{O}(1) & \mathcal{O}(1) & 0 \\ \mathcal{O}(1) & \mathcal{O}(1) & \mathcal{O}(1) \\ \mathcal{O}(1) & \mathcal{O}(1) & \mathcal{O}(1) \end{bmatrix}$$

$$\text{VPIE-2:} \begin{bmatrix} \mathbf{Z}_{LL} & \mathbf{Z}_{LS} & \mathbf{Z}_{LP} \\ \mathbf{Z}_{SL} & \mathbf{Z}_{SS} & \mathbf{Z}_{SP} \\ \mathbf{Z}_{PL} & \mathbf{Z}_{PS} & \mathbf{Z}_{PP} \end{bmatrix} = \begin{bmatrix} \mathcal{O}(1) & \mathcal{O}(1) & 0 \\ \mathcal{O}(1) & \mathcal{O}(1) & \mathcal{O}(1) \\ 0 & \mathcal{O}(1) & \mathcal{O}(\omega^2) \end{bmatrix}. \quad (27)$$

Consequently, the scaling of the inverses of these matrices can be found using the Schur complement [35]

$$\text{VPIE-1:} \begin{bmatrix} \mathbf{Z}_{LL} & \mathbf{Z}_{LS} & \mathbf{Z}_{LP} \\ \mathbf{Z}_{SL} & \mathbf{Z}_{SS} & \mathbf{Z}_{SP} \\ \mathbf{Z}_{PL} & \mathbf{Z}_{PS} & \mathbf{Z}_{PP} \end{bmatrix}^{-1} = \begin{bmatrix} \mathcal{O}(1) & \mathcal{O}(1) & \mathcal{O}(1) \\ \mathcal{O}(1) & \mathcal{O}(1) & \mathcal{O}(1) \\ \mathcal{O}(1) & \mathcal{O}(1) & \mathcal{O}(1) \end{bmatrix}$$

$$\text{VPIE-2:} \begin{bmatrix} \mathbf{Z}_{LL} & \mathbf{Z}_{LS} & \mathbf{Z}_{LP} \\ \mathbf{Z}_{SL} & \mathbf{Z}_{SS} & \mathbf{Z}_{SP} \\ \mathbf{Z}_{PL} & \mathbf{Z}_{PS} & \mathbf{Z}_{PP} \end{bmatrix}^{-1} = \begin{bmatrix} \mathcal{O}(1) & \mathcal{O}(\omega^2) & \mathcal{O}(1) \\ \mathcal{O}(\omega^2) & \mathcal{O}(\omega^2) & \mathcal{O}(1) \\ \mathcal{O}(1) & \mathcal{O}(1) & \mathcal{O}(1) \end{bmatrix}. \quad (28)$$

On the other hand, the scaling of the right-hand side vectors $\mathbf{V}_L$, $\mathbf{V}_S$, and $\mathbf{V}_P$ depends on the selection of $\mathbf{A}^{\text{inc}}(\mathbf{r})$ and $\Phi^{\text{inc}}(\mathbf{r})$. Assume that the electric field of the plane-wave excitation is expressed as $\mathbf{E}^{\text{inc}}(\mathbf{r}) = \mathbf{E}_0 e^{-jk_0 \hat{\mathbf{k}}^{\text{inc}} \cdot \mathbf{r}}$, where $\mathbf{E}_0$ is the polarization vector. As frequency approaches zero, $\mathbf{E}^{\text{inc}}(\mathbf{r})$ scales as $\mathcal{O}(1)$ [4]. Using this, one can easily see from (26) that $\mathbf{V}_S$ scales as $\mathcal{O}(\omega^{-1})$ and $\mathcal{O}(1)$ with the first and second kinds of potential representations, respectively. The scaling of $\mathbf{V}_P$ depends not only on the kind of potential representations but also on the choice of VPIE. It can be seen from (14) that $\mathbf{V}_P$ scales as $\mathcal{O}(\omega^{-1})$ and $\mathcal{O}(1)$ for VPIE-1 with the first and second potential representations, respectively, and as $\mathcal{O}(\omega)$ for VPIE-2 with the second potential representation. Note that $\Phi_1^{\text{inc}}(\mathbf{r}) = 0$ ensures $\mathbf{V}_P = 0$ for VPIE-2 with the first potential representation. On the other hand, derivation of the scaling of $\mathbf{V}_L$ calls for a more involved investigation as described next. The loop basis function $\mathbf{f}_m^L(\mathbf{r})$ can be expressed as [36]

$$\mathbf{f}_m^L(\mathbf{r}) = \hat{\mathbf{n}}(\mathbf{r}) \times \nabla_s \varphi_m(\mathbf{r}) \quad (29)$$

where $\varphi_m(\mathbf{r})$ is a pyramid-shaped function defined at $\mathbf{r} \in \Gamma_m^L$, and ∇_s denotes the surface gradient. Inserting (29) into (25) with two kinds of potential representations and using the chain rule and the divergence theorem in the resulting expressions yield [7]

$$\{\mathbf{V}_L\}_m = \frac{-1}{j\omega} \left\{ -jk_0 \int_{\Gamma_m^L} \varphi_m(\mathbf{r}) \hat{\mathbf{n}}(\mathbf{r}) \cdot [\hat{\mathbf{k}}^{\text{inc}} \times \mathbf{E}^{\text{inc}}(\mathbf{r})] ds \right.$$

$$\left. + \oint_{\partial \Gamma_m^L} \hat{\mathbf{m}}(\mathbf{r}) \cdot [\varphi_m(\mathbf{r}) \hat{\mathbf{n}}(\mathbf{r}) \times \mathbf{E}^{\text{inc}}(\mathbf{r})] dl \right\}$$

$$= \sqrt{\mu_0 \varepsilon_0} \int_{\Gamma_m^L} \varphi_m(\mathbf{r}) \hat{\mathbf{n}}(\mathbf{r}) \cdot [\hat{\mathbf{k}}^{\text{inc}} \times \mathbf{E}^{\text{inc}}(\mathbf{r})] ds \quad (30)$$

$$\{\mathbf{V}_L\}_m = -\sqrt{\mu_0 \varepsilon_0} \left\{ \int_{\Gamma_m^L} \varphi_m(\mathbf{r}) \hat{\mathbf{n}}(\mathbf{r}) \cdot \left[\nabla \times (\hat{\mathbf{k}}^{\text{inc}} (\mathbf{r} \cdot \mathbf{E}^{\text{inc}}(\mathbf{r}))) \right] ds \right.$$

$$+ \oint_{\partial \Gamma_m^L} \hat{\mathbf{m}}(\mathbf{r}) \cdot \left[\varphi_m(\mathbf{r}) \hat{\mathbf{n}}(\mathbf{r}) \right.$$

$$\left. \times (\hat{\mathbf{k}}^{\text{inc}} (\mathbf{r} \cdot \mathbf{E}^{\text{inc}}(\mathbf{r}))) \right] dl \Bigg\}$$

$$= -\sqrt{\mu_0 \varepsilon_0} \int_{\Gamma_m^L} \varphi_m(\mathbf{r}) \hat{\mathbf{n}}(\mathbf{r})$$

$$\cdot \left[e^{-jk_0 \hat{\mathbf{k}}^{\text{inc}} \cdot \mathbf{r}} \nabla \times (\hat{\mathbf{k}}^{\text{inc}} (\mathbf{r} \cdot \mathbf{E}_0)) \right.$$

$$\left. - (\hat{\mathbf{k}}^{\text{inc}} (\mathbf{r} \cdot \mathbf{E}_0)) \times \nabla e^{-jk_0 \hat{\mathbf{k}}^{\text{inc}} \cdot \mathbf{r}} \right] ds$$

$$= \sqrt{\mu_0 \varepsilon_0} \int_{\Gamma_m^L} \varphi_m(\mathbf{r}) \hat{\mathbf{n}}(\mathbf{r}) \cdot \left[e^{-jk_0 \hat{\mathbf{k}}^{\text{inc}} \cdot \mathbf{r}} (\hat{\mathbf{k}}^{\text{inc}} \times \mathbf{E}_0) \right] ds \quad (31)$$

for $(\mathbf{A}_1^{\text{inc}}, \Phi_1^{\text{inc}})$ and $(\mathbf{A}_2^{\text{inc}}, \Phi_2^{\text{inc}})$, respectively. Here, $\hat{\mathbf{m}}(\mathbf{r})$ denotes the unit normal vector pointing outward on $\partial \Gamma_m^L$, the boundary of Γ_m^L. Since $\varphi_m(\mathbf{r}) = 0$ on $\partial \Gamma_m^L$ [36], the contour integrals in (30) and (31) are zero. Since $\mathbf{E}^{\text{inc}}(\mathbf{r})$ scales as $\mathcal{O}(1)$ [4], one can show that $\mathbf{V}_L$ scales as $\mathcal{O}(1)$ for both the representations of the incident plane wave. In summary, one obtains

$$\text{VPIE-1:} \begin{bmatrix} \mathbf{V}_L \\ \mathbf{V}_S \\ \mathbf{V}_P \end{bmatrix} = \begin{cases} \left[\mathcal{O}(1) \, \mathcal{O}(\omega^{-1}) \, \mathcal{O}(\omega^{-1}) \right]^T, & \left(\mathbf{A}_1^{\text{inc}}, \Phi_1^{\text{inc}} \right) \\ \left[\mathcal{O}(1) \, \mathcal{O}(1) \, \mathcal{O}(1) \right]^T, & \left(\mathbf{A}_2^{\text{inc}}, \Phi_2^{\text{inc}} \right) \end{cases}$$

$$\text{VPIE-2:} \begin{bmatrix} \mathbf{V}_L \\ \mathbf{V}_S \\ \mathbf{V}_P \end{bmatrix} = \begin{cases} \left[\mathcal{O}(1) \, \mathcal{O}(\omega^{-1}) \, 0 \right]^T, & \left(\mathbf{A}_1^{\text{inc}}, \Phi_1^{\text{inc}} \right) \\ \left[\mathcal{O}(1) \, \mathcal{O}(1) \, \mathcal{O}(\omega) \right]^T, & \left(\mathbf{A}_2^{\text{inc}}, \Phi_2^{\text{inc}} \right). \end{cases} \quad (32)$$

Finally, multiplying (28) with (32) yields the frequency scaling of $\mathbf{I}_L$, $\mathbf{I}_S$, and $\mathbf{I}_P$ in (16) as

$$\text{VPIE-1:} \begin{bmatrix} \mathbf{I}_L \\ \mathbf{I}_S \\ \mathbf{I}_P \end{bmatrix} = \begin{cases} \left[\mathcal{O}(\omega^{-1}) \, \mathcal{O}(\omega^{-1}) \, \mathcal{O}(\omega^{-1}) \right]^T, & \left(\mathbf{A}_1^{\text{inc}}, \Phi_1^{\text{inc}} \right) \\ \left[\mathcal{O}(1) \, \mathcal{O}(1) \, \mathcal{O}(1) \right]^T, & \left(\mathbf{A}_2^{\text{inc}}, \Phi_2^{\text{inc}} \right) \end{cases}$$

$$\text{VPIE-2:} \begin{bmatrix} \mathbf{I}_L \\ \mathbf{I}_S \\ \mathbf{I}_P \end{bmatrix} = \begin{cases} \left[\mathcal{O}(1) \, \mathcal{O}(\omega) \, \mathcal{O}(\omega^{-1}) \right]^T, & \left(\mathbf{A}_1^{\text{inc}}, \Phi_1^{\text{inc}} \right) \\ \left[\mathcal{O}(1) \, \mathcal{O}(\omega) \, \mathcal{O}(1) \right]^T, & \left(\mathbf{A}_2^{\text{inc}}, \Phi_2^{\text{inc}} \right). \end{cases} \quad (33)$$

One can expect that the scaling of $\mathbf{I}_P$ (which stores expansion coefficients of $\hat{\mathbf{n}} \cdot \mathbf{A}$) should be different under different representations of the excitation. But this should not be the case for $\mathbf{I}_L$ and $\mathbf{I}_S$ (which store the expansion coefficients of $\mathbf{J}$) since the field representation of the excitation is unique. Having said that, the correct frequency scaling of $\mathbf{I}_L$ and $\mathbf{I}_S$ has been discussed in [4] and [21] and is shown to be $\mathcal{O}(1)$ and $\mathcal{O}(\omega)$, respectively. These results are obtained from the asymptotic solution of EFIE or MFIE as $\omega \to 0$. The latter can also be seen easily from the current continuity equation [4], [21].

Looking at (33), one can see that the scaling of $\mathbf{I}_L$ and $\mathbf{I}_S$ obtained by solving VPIE-2 is correct but the same cannot be said for those obtained by solving VPIE-1. Indeed, this conclusion is supported by the numerical results presented in Section III. Note that since (the scaling of) $\mathbf{I}_P$ depends on the potential representation of the excitation, one has to be careful while computing the scattered fields from the solution of VPIE-2 as $\omega \to 0$ [28].

III. NUMERICAL RESULTS

In this section, low-frequency behavior of VPIE-1 and VPIE-2 is investigated via numerical experiments. In all the simulations, the scatterer is a PEC unit sphere that resides in free space and is centered at the origin. The excitation is a plane wave with electric field $\mathbf{E}^{\text{inc}}(\mathbf{r}) = \hat{\mathbf{x}} e^{-jk_0 z}$. The surface of the sphere is discretized using $N_P = 2560$ triangular patches resulting in $N_R = 3840$ edges. The deflation method [20] is applied to the VPIE-2 matrix system when the frequency is smaller than 1 KHz. The LU decomposition is used to solve the matrix systems in (8) (for VPIE-1 and VPIE-2) and the matrix system is modified by deflation (for VPIE-2) to ensure that the error in the matrix solution is at the machine precision level.

A. Accuracy of VPIE-1 and VPIE-2

In this section, the accuracy of VPIE-1 and VPIE-2 is investigated by comparing the radar cross section (RCS) of the unit sphere computed using $\mathbf{I}_R$ after solving VPIE-1 and VPIE-2 (for two kinds of potential representations of the incident plane wave) to RCS computed using the Mie series solution [37]. Fig. 1(a) and (b) show plots of RCS for $\theta = [0°, 180°]$ and $\phi = 0°$ at 300 MHz and 0.1 Hz, respectively. Fig. 1(a) shows that RCS computed using VPIE-1 and
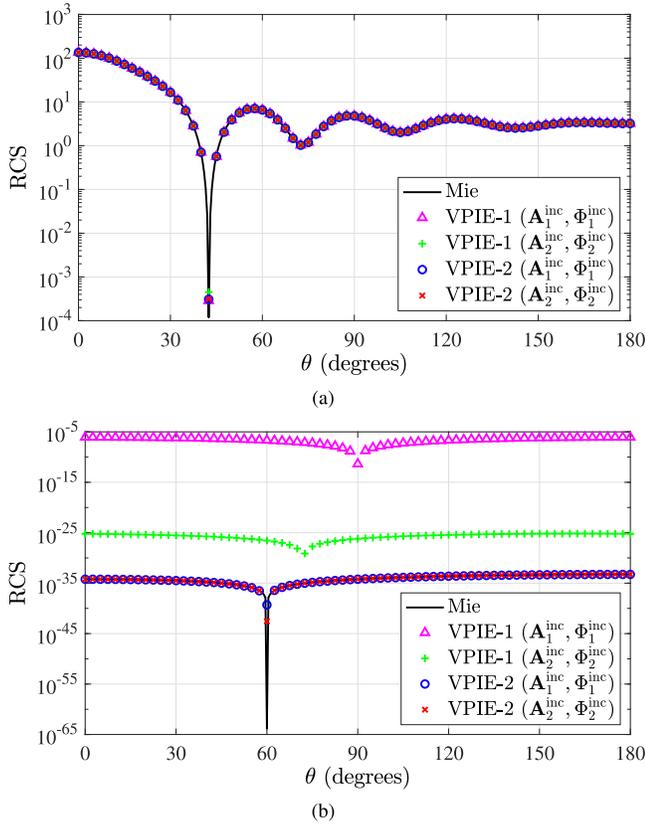
(a)

(b)

Fig. 1. RCS computed using VPIE-1 and VPIE-2 solutions with two potential representations of the incident plane wave and the Mie series solution for $\theta = [0°, 180°]$ and $\phi = 0°$ at (a) 300 MHz and (b) 0.1 Hz.

VPIE-2 solutions at 300 MHz matches very well to RCS computed using the Mie series solution (for both the representations of the excitation). However, as shown in Fig. 1(b), at 0.1 Hz, only RCS computed using the VPIE-2 solution agrees well with RCS computed using the Mie series solution. The L_2-norm RCS error values of VPIE-2 are 8.24×10^{-3} and 8.52×10^{-3} for the first and second representations of the excitation, respectively. VPIE-1 solution is not accurate for neither representation of the excitation. This result agrees with the conclusion of the analysis carried out in Section II-D: the electric current obtained by solving VPIE-1 is not accurate at low frequencies while that obtained by solving VPIE-2 maintains its accuracy. Fig. 1(b) also shows that the L_2-norm RCS error of VPIE-1 with the first representation of the excitation (1.96×10^{27}) is larger than that of VPIE-1 with the second representation of the excitation (1.54×10^8). This might be explained by the fact that the vector potential used in the first representation becomes unbounded as $\omega \to 0$. Indeed, as shown in Section III-B, both $\mathbf{I}_L$ and $\mathbf{I}_S$ obtained from the solution of VPIE-1 with the first representation follow the behavior of the vector potential of the excitation and also become unbounded. This increases the RCS error [4].

B. Frequency Scaling of VPIE-1 and VPIE-2 Solutions

In this section, the frequency scaling of $\mathbf{I}_L$, $\mathbf{I}_S$, and $\mathbf{I}_P$ obtained from the VPIE-1 and VPIE-2 solutions as $\omega \to 0$ is numerically investigated. The frequency is swept in the interval [0.01 Hz, 300 MHz]. Note that $\mathbf{I}_L$ and $\mathbf{I}_S$ are not obtained by directly solving (16). First (8) (for VPIE-1 and VPIE-2) and the matrix system modified by deflation (for VPIE-2) are solved for $\mathbf{I}_R$, and then $\mathbf{I}_L$ and $\mathbf{I}_S$ are obtained from $\mathbf{I}_R$ via postprocessing [11]. Fig. 2(a)–(c) show the plots of the L_2-norm of $\mathbf{I}_L$, $\mathbf{I}_S$, and $\mathbf{I}_P$ versus the frequency
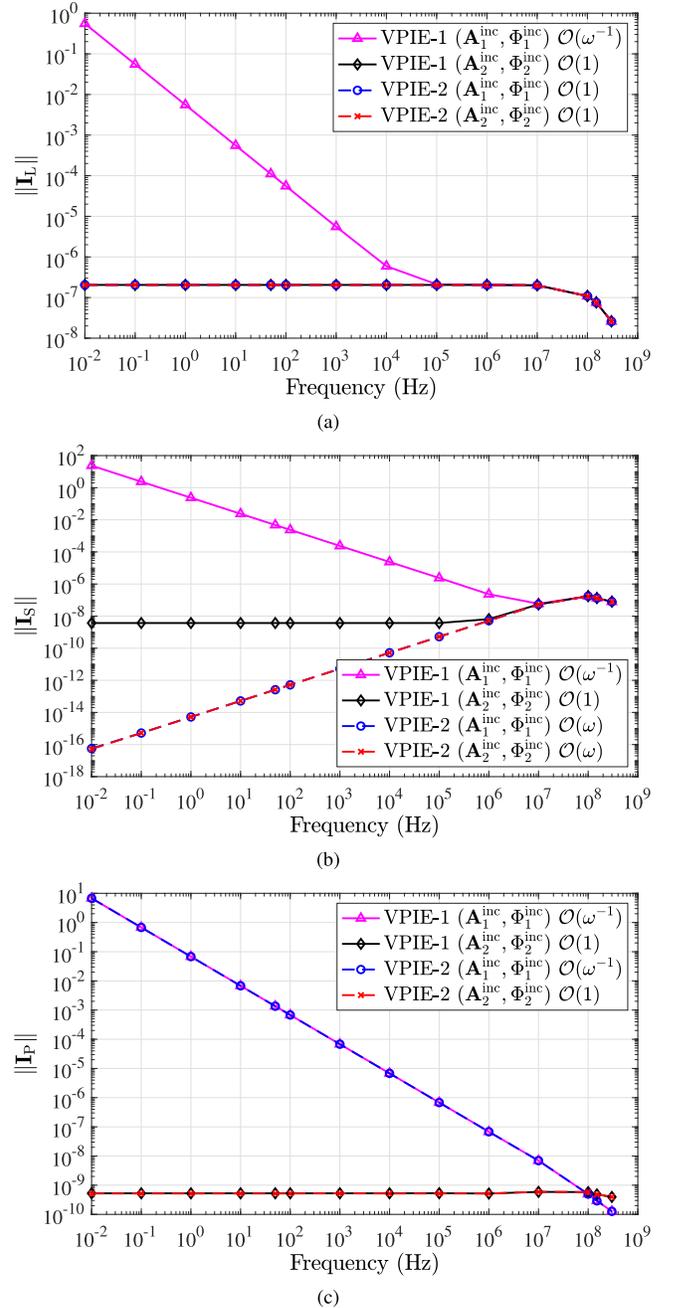

(a)

(b)

(c)

Fig. 2. L_2-norm of (a) $\mathbf{I}_L$, (b) $\mathbf{I}_S$, and (c) $\mathbf{I}_P$ versus the frequency for VPIE-1 and VPIE-2 with two different potential representations of the incident plane wave.

for VPIE-1 and VPIE-2 with both the potential representations of the incident plane wave, respectively. Fig. 2(a) clearly shows that $\|\mathbf{I}_L\|$ obtained from the solution of VPIE-1 with the first and second representations scales as $\mathcal{O}(\omega^{-1})$ and $\mathcal{O}(1)$ as $\omega \to 0$, respectively. $\|\mathbf{I}_L\|$ obtained from the solution of VPIE-2 with both the representations scales as $\mathcal{O}(1)$ as $\omega \to 0$. As shown in Fig. 2(b), $\|\mathbf{I}_S\|$ obtained from the solution of VPIE-1 with the first and second representations scales as $\mathcal{O}(\omega^{-1})$ and $\mathcal{O}(1)$, respectively, and $\|\mathbf{I}_S\|$ obtained from the solution of VPIE-2 with both the representations scales as $\mathcal{O}(\omega)$. Fig. 2(c) shows that $\|\mathbf{I}_P\|$ obtained from the solutions of VPIE-1 and VPIE-2 with the first representation scales as $\mathcal{O}(\omega^{-1})$, while $\|\mathbf{I}_P\|$ obtained with the second representation scales as $\mathcal{O}(1)$. The results presented in Fig. 2 support the conclusions of the analysis carried out in Section II-D: the scaling of the electric current solution

of VPIE-2 follows the theoretical prediction, while that of VPIE-1 does not, and this applies to both the representations of the incident plane wave. In addition, the scaling of the solution for the normal component of the vector potential depends only on the representation of the incident plane wave.

IV. CONCLUSION

The low-frequency behavior of VPIEs for PEC scatterers is investigated. Two equation sets are considered: VPIE-1 enforces the tangential component of the vector potential on the scatterer surface to be zero and also uses the fundamental field relationship on its normal component, and VPIE-2 uses the same condition as VPIE-1 for the tangential component of the vector potential but enforces its divergence to be zero. To numerically solve VPIE-1 and VPIE-2, the electric current and the normal component of the vector potential on the surface of the scatterer are expanded using the RWG and pulse basis functions, respectively. VPIE-1 is tested using the RWG and scalar BC functions, while VPIE-2 is tested using the RWG and pulse functions. Theoretical analysis carried out using loop–star decomposition on the resulting matrix equations, and numerical experiments show that the electric current obtained by solving VPIE-1 has the wrong frequency scaling and is inaccurate at low frequencies.

This work considers only simply connected scatterers. The low-frequency behavior of VPIEs enforced on nonsimply connected surfaces will be theoretically and numerically analyzed in future work.

REFERENCES

[1] S. M. Rao, D. R. Wilton, and A. W. Glisson, "Electromagnetic scattering by surfaces of arbitrary shape," *IEEE Trans. Antennas Propag.*, vol. AP-30, no. 3, pp. 409–418, Mar. 1982.

[2] F. P. Andriulli, A. Tabacco, and G. Vecchi, "Solving the EFIE at low frequencies with a conditioning that grows only logarithmically with the number of unknowns," *IEEE Trans. Antennas Propag.*, vol. 58, no. 5, pp. 1614–1624, May 2010.

[3] Z. G. Qian and W. C. Chew, "A quantitative study on the low frequency breakdown of EFIE," *Microw. Opt. Technol. Lett.*, vol. 50, no. 5, pp. 1159–1162, May 2008.

[4] Y. Zhang, T. J. Cui, W. C. Chew, and J.-S. Zhao, "Magnetic field integral equation at very low frequencies," *IEEE Trans. Antennas Propag.*, vol. 51, no. 8, pp. 1864–1871, Aug. 2003.

[5] K. Cools, F. P. Andriulli, D. D. Zutter, and E. Michielssen, "Accurate and conforming mixed discretization of the MFIE," *IEEE Antennas Wireless Propag. Lett.*, vol. 10, pp. 528–531, 2011.

[6] I. Bogaert, K. Cools, F. P. Andriulli, and H. Bagci, "Low-frequency scaling of the standard and mixed magnetic field and Müller integral equations," *IEEE Trans. Antennas Propag.*, vol. 62, no. 2, pp. 822–831, Feb. 2014.

[7] H. A. Ulku, I. Bogaert, K. Cools, F. P. Andriulli, and H. Bagci, "Mixed discretization of the time-domain MFIE at low frequencies," *IEEE Antennas Wireless Propag. Lett.*, vol. 16, pp. 1565–1568, 2017.

[8] G. Vecchi, "Loop-star decomposition of basis functions in the discretization of the EFIE," *IEEE Trans. Antennas Propag.*, vol. 47, no. 2, pp. 339–346, Feb. 1999.

[9] J.-S. Zhao and W. C. Chew, "Integral equation solution of Maxwell's equations from zero frequency to microwave frequencies," *IEEE Trans. Antennas Propag.*, vol. 48, no. 10, pp. 1635–1645, Oct. 2000.

[10] S. Yan, J.-M. Jin, and Z. Nie, "EFIE analysis of low-frequency problems with loop-star decomposition and Calderón multiplicative preconditioner," *IEEE Trans. Antennas Propag.*, vol. 58, no. 3, pp. 857–867, Mar. 2010.

[11] F. P. Andriulli, "Loop-star and loop-tree decompositions: Analysis and efficient algorithms," *IEEE Trans. Antennas Propag.*, vol. 60, no. 5, pp. 2347–2356, May 2012.

[12] J. Cheng and R. J. Adams, "Electric field-based surface integral constraints for Helmholtz decompositions of the current on a conductor," *IEEE Trans. Antennas Propag.*, vol. 61, no. 9, pp. 4632–4640, Sep. 2013.

[13] S. H. Christiansen and J.-C. Nédélec, "A preconditioner for the electric field integral equation based on Calderon formulas," *SIAM J. Numer. Anal.*, vol. 40, no. 3, pp. 1100–1135, 2001.

[14] A. Buffa and S. Christiansen, "A dual finite element complex on the barycentric refinement," *Math. Comput.*, vol. 76, no. 260, pp. 1743–1769, May 2007.

[15] M. A. E. Bautista, M. A. Francavilla, F. Vipiana, and G. Vecchi, "A hierarchical fast solver for EFIE-MoM analysis of multiscale structures at very low frequencies," *IEEE Trans. Antennas Propag.*, vol. 62, no. 2, pp. 1523–1528, Mar. 2014.

[16] F. P. Andriulli et al., "A multiplicative Calderón preconditioner for the electric field integral equation," *IEEE Trans. Antennas Propag.*, vol. 56, no. 8, pp. 2398–2412, Aug. 2008.

[17] M. B. Stephanson and J.-F. Lee, "Preconditioned electric field integral equation using Calderón identities and dual loop/star basis functions," *IEEE Trans. Antennas Propag.*, vol. 57, no. 4, pp. 1274–1279, Apr. 2009.

[18] S. Sun, Y. G. Liu, W. C. Chew, and Z. Ma, "Calderón multiplicative preconditioned EFIE with perturbation method," *IEEE Trans. Antennas Propag.*, vol. 61, no. 1, pp. 247–255, Jan. 2013.

[19] M. Taskinen and P. Ylä-Oijala, "Current and charge integral equation formulation," *IEEE Trans. Antennas Propag.*, vol. 54, no. 1, pp. 58–67, Jan. 2006.

[20] Z.-G. Qian and W. C. Chew, "Fast full-wave surface integral equation solver for multiscale structure modeling," *IEEE Trans. Antennas Propag.*, vol. 57, no. 11, pp. 3594–3601, Nov. 2009.

[21] Z.-G. Qian and W. C. Chew, "Enhanced A-EFIE with perturbation method," *IEEE Trans. Antennas Propag.*, vol. 58, no. 10, pp. 3256–3264, Oct. 2010.

[22] J. Cheng, R. J. Adams, J. C. Young, and M. A. Khayat, "Augmented EFIE with normally constrained magnetic field and static charge extraction," *IEEE Trans. Antennas Propag.*, vol. 63, no. 11, pp. 4952–4963, Nov. 2015.

[23] F. Vico, L. Greengard, M. Ferrando, and Z. Gimbutas, "The decoupled potential integral equation for time-harmonic electromagnetic scattering," *Commun. Pure Appl. Math.*, vol. 69, no. 4, pp. 771–812, Apr. 2016.

[24] W. C. Chew, "Vector potential electromagnetics with generalized gauge for inhomogeneous media: Formulation (invited paper)," *Prog. Electromagn. Res.*, vol. 149, pp. 69–84, 2014.

[25] Q. S. Liu, S. Sun, and W. C. Chew, "A vector potential integral equation method for electromagnetic scattering," in *Proc. Int. Rev. Prog. Appl. Comput. Electromagn. (ACES)*, Williamsburg, VA, USA, Mar. 2015, pp. 1–2.

[26] Q. S. Liu, S. Sun, and W. C. Chew, "A potential-based integral equation method for low-frequency electromagnetic problems," *IEEE Trans. Antennas Propag.*, vol. 66, no. 3, pp. 1413–1426, Mar. 2018.

[27] J. Li, X. Fu, and B. Shanker, "Decoupled potential integral equations for electromagnetic scattering from dielectric objects," *IEEE Trans. Antennas Propag.*, vol. 67, no. 3, pp. 1729–1739, Mar. 2019.

[28] U. M. Gür and Ö. Ergül, "Accuracy of sources and near-zone fields when using potential integral equations at low frequencies," *IEEE Antennas Wireless Propag. Lett.*, vol. 16, pp. 2783–2786, 2017.

[29] T. E. Roth and W. C. Chew, "Development of stable A-Φ time domain integral equations for multiscale electromagnetics," *IEEE J. Multiscale Multiphys. Comput. Tech.*, vol. 3, pp. 255–265, 2018.

[30] T. E. Roth and W. C. Chew, "Stability analysis and discretization of A-Φ time domain integral equations for multiscale electromagnetics," *J. Comput. Phys.*, vol. 408, May 2020, Art. no. 109102.

[31] T. E. Roth and W. C. Chew, "Lorenz gauge potential-based time domain integral equations for analyzing subwavelength penetrable regions," *IEEE J. Multiscale Multiphys. Comput. Techn.*, vol. 6, pp. 24–34, 2021.

[32] R. Chen and H. Bagci, "On the low-frequency scaling of vector potential integral equation solutions," in *Proc. IEEE Int. Symp. Antennas Propag. USNC-URSI Radio Sci. Meeting (APS/URSI)*, Singapore, Dec. 2021, pp. 431–432.

[33] M. Benzi, G. H. Golub, and J. Liesen, "Numerical solution of saddle point problems," *Acta Numer.*, vol. 14, pp. 1–137, Apr. 2005.

[34] R. Mitharwal and F. P. Andriulli, "On the multiplicative regularization of graph Laplacians on closed and open structures with applications to spectral partitioning," *IEEE Access*, vol. 2, pp. 788–796, 2014.

[35] F. Zhang, *The Schur Complement and Its Applications*. Berlin, Germany: Springer, 2006, pp. 1–295.

[36] S. Y. Chen, W. C. Chew, J. M. Song, and J.-S. Zhao, "Analysis of low frequency scattering from penetrable scatterers," *IEEE Trans. Geosci. Remote Sens.*, vol. 39, no. 4, pp. 726–735, Apr. 2001.

[37] J.-M. Jin, *Theory and Computation of Electromagnetic Fields*. Hoboken, NJ, USA: Wiley, 2010, pp. 1–572.